Available online at www.sciencedirect.com
ScienceDirect
Journal of Catalysis 246 (2007) 52–59
JOURNAL OF CATALYSIS
www.elsevier.com/locate/jcat

High-surface area CuO–CeO_2 catalysts prepared by a surfactant-templated method for low-temperature CO oxidation

Meng-Fei Luo *, Jing-Meng Ma, Ji-Qing Lu, Yu-Peng Song, Yue-Juan Wang

Zhejiang Key Laboratory for Reactive Chemistry on Solid Surfaces, Institute of Physical Chemistry, Zhejiang Normal University, Jinhua 321004, China

Received 10 September 2006; revised 22 November 2006; accepted 22 November 2006

Available online 21 December 2006

Abstract

High-surface area nanosized CuO–CeO_2 catalysts were prepared by a surfactant-templated method and tested for CO oxidation. The catalysts were characterized by XRD, TEM, N_2 sorption, H_2-TPR, and CO-TPR. The surfactant method can be used for preparing CuO–CeO_2 mixed oxides with a crystallite size of about 5 nm. The highest BET surface area of the catalysts was 215 $m^2\,g^{-1}$, achieved over a 3.3% CuO content catalyst. XRD results indicated that the absence of a CuO phase with <12% CuO content may partially incorporate in the CeO_2 lattice to form $Cu_xCe_{1-x}O_{2-\delta}$ solid solution, whereas a higher CuO content causes the formation of bulk CuO. These high-surface area nanosized catalysts were found to be very active for CO oxidation reaction; the lowest T_{90} was 80 °C, achieved over a 12.0% CuO content catalyst. In addition, the CuO–CeO_2 catalysts also show high catalytic activity for selective oxidation of CO in excess H_2 at relatively low temperature. H_2-TPR results reveal three reduction peaks for these catalysts, which could be attributed to reduction of the highly dispersed CuO, the Cu^{2+} in the CeO_2 lattice, and the bulk CuO. Removal of the finely dispersed CuO in the catalyst by acid treatment resulted in a decline in catalytic activity for CO oxidation, indicating that the finely dispersed CuO species are the active sites for the reaction.

Keywords: CO oxidation; CuO–CeO_2; Surface area; Catalytic activity

1. Introduction

Cerium dioxide powders have potential applications in polishing powders, coatings for high-temperature optical and ceramic materials, and gas sensors [1]. Because of its low temperature reducibility, oxygen storage, and release properties, ceria is also widely used as a support for many oxidation catalysts. These catalysts are active in oxidation of CO [2], water–gas shift reactions [3], elimination of CO and NO_x contaminants from automotive exhaust gases, combustion of hydrocarbons [4], and other reactions. One of the most important applications of ceria is its use as an additive in the three-way catalysts for automotive exhaust gas treatment. The interaction of ceria with precious metals (Pd, Pt, Rh) and its effect on catalytic activity are well documented [5,6].

Although precious metal catalysts have high activity and desirable air and temperature stability, their high cost may limit their application. Recent reports have shown that the activity of Ce-related oxides in total oxidation reactions is greatly enhanced not only by noble metals, but also by transitional metals like copper, and the CeO_{2-x}-supported CuO catalyst is comparable or superior to platinum catalysts for the preferential oxidation of CO in excess hydrogen [7–9]. The promoting effect had been correlated with the synergism of the redox properties of the system, which is achieved by the formation of copper–ceria interactions, with both components being significantly more readily reduced or oxidized than the corresponding independent components [10].

Varying the preparation routes often leads to changes in the morphology and dispersion of copper species. Methods in current use include co-precipitation [11], deposition–precipitation, impregnation [12], sol–gel, and urea methods [13]. We have previously reported [14] the synthesis of CuO/CeO_2 by an impregnation method. The catalysts exhibit high catalytic activities in CO oxidation. The activity is close to that of the

* Corresponding author. Fax: +86 579 2282595.
E-mail address: mengfeiluo@zjnu.cn (M.-F. Luo).

0021-9517/$ – see front matter
doi:10.1016/j.jcat.2006.11.021

Au/MnO_x catalyst and clearly superior to that of the Pt/SnO_x catalyst reported in the literature [15]. Increasing the surface area and reducing the particle size to nanoscale will provide numerous, more reactive sites [16] so as to enhance the catalyst activity. Several routes for synthesizing nanosized ceria and cerium-based mixed oxides have been investigated. Hirano and Inagaki [17] obtained fine CeO_2 from $Ce(NO_3)_3$, $Ce(SO_4)_2$, and $Ce(NH_4)_4(SO_4)_4$ solutions at 180 °C under autogenous pressure. Tok et al. [18] reported the synthesis of Gd_2O_3-doped CeO_2 solid solution nanoparticles via carbonate co-precipitation. Skårman et al. [19] obtained nanostructured CuO_x/CeO_2 composites by inert gas condensation (IGC). Shen et al. [20] reported the synthesis of CuO-loaded mesoporous CeO_2 using the ordered mesoporous silica KIT-6 as a hard template. The surface area of the catalyst with 20% CuO loading was 88 $m^2\,g^{-1}$, and a T_{50} of 116 °C was obtained for the CO oxidation reaction.

In this paper, a series of high-surface area nanosized CuO–CeO_2 catalysts were prepared by a surfactant-templated method, and their catalytic performance was tested for the CO oxidation reaction. The active phase for CO oxidation was also investigated.

2. Experimental

2.1. Catalyst preparation

The CuO–CeO_2 catalysts with different CuO content (3.3, 6.1, 12.0, 28.3, 50.1 mol%) were prepared using a surfactant-templated method. For a typical synthesis, cetyltrimethyl ammonium bromide (CTAB; 6 mmol) was dissolved in 200 mL of distilled water, followed by the addition of $Ce(NO_3)_3{\cdot}6H_2O$ (9.5 mmol) and $Cu(NO_3)_2{\cdot}3H_2O$ (5 mmol). The mixture was stirred for 0.5 h, after which a solution of sodium hydroxide (50 mmol) in 300 mL of distilled water was added and stirred for 12 h. The final precipitate was aged at 90 °C for 3 h, washed with hot water, dried at 110 °C for 6 h, and finally calcined at 400 °C for 4 h. Other catalysts with different CuO contents were prepared in a similar manner. The actual CuO content in the catalyst was analyzed by atomic absorption spectrophotometry (AAS); for example, a CeCu3 catalyst means a CuO–CeO catalyst with CuO content of 3.3 mol%. It was found the actual CuO content (3.3 mol%) was lower than the CuO content in the starting solution (5 mol%).

For comparison, CuO/SiO_2 and $CuO/\gamma\text{-}Al_2O_3$ catalysts were prepared by an incipient wetness method. A SiO_2 (BET area, 730 $m^2\,g^{-1}$) or $\gamma\text{-}Al_2O_3$ (BET area, 212 $m^2\,g^{-1}$) support was immerged with a proper amount of $Cu(NO_3)_2{\cdot}3H_2O$ solution for 4 h. The slurry was heated at 80 °C to remove the water and dried at 100 °C for 7 h, followed by calcination at 400 °C for 4 h in air. The CuO content in these catalysts was 12 mol%. Pure CuO and CeO_2 were prepared by decomposition of $Cu(NO_3)_2{\cdot}3H_2O$ and $Ce(NO_3)_3{\cdot}6H_2O$ at 400 °C for 4 h in air. In addition, a series of Ce–Cu–O catalysts with 10 mol% CuO content were prepared according to the typical method reported in the literature [21]. The sample directly calcined in air at 400 or 800 °C was designated as A4 or A8, respectively. The sample heated in N_2 at 800 °C was designated as N8. The N8 sample followed by calcinations in air at 400 °C was designated as N8A4.

2.2. Characterizations

X-ray diffraction (XRD) patterns were collected on a PHILIPS PW 3040/60 powder diffractometer using Cu$K\alpha$ radiation. The working voltage was 40 kV, and the current was 40 mA. The intensity data were collected at 25 °C in a 2θ range of 20°–130° with a scan rate of 1.2° min^{-1}. The microstructural parameters of samples were determined by the Rietveld method [22] using MAUD software (material analysis using diffraction) [23]. CeO_2 annealed at 1450 °C for 10 h in air was used as a nonintrinsic broadening sample to measure the instrument function and to extract the microstructure values of the catalyst.

N_2 sorption isotherms were obtained at 77 K on an Autosorb-1 apparatus. BET and BJH analysis were used to determine the surface area and pore size distribution of the samples. Transmission electron microscopy (TEM) observations were made using a JEM2010 microscope operated at 200 kV. X-ray photon spectroscopy (XPS) experiments were carried out on a RBD upgraded PHI-5000C ESCA system (Perkin-Elmer) with Mg$K\alpha$ radiation ($h\nu = 1253.6$ eV). The pass energy was fixed at 46.95 eV to ensure sufficient sensitivity. Binding energies were calibrated by using the containment carbon (C1s = 284.6 eV). The data analysis was performed using the RBD AugerScan 3.21 software (RBD Enterprises).

The reduction properties of CuO–CeO_2 catalysts were measured by temperature-programmed reduction (TPR) techniques, including H_2-TPR and CO-TPR. A 10-mg sample was placed in a quartz reactor connected to a homemade TPR apparatus, and the reactor was heated from 100 to 900 °C at a rate of 20 °C min^{-1}. The amount of H_2 uptake during the reduction was measured using a thermal conductivity detector (TCD), and the amount of CO_2 desorbed during the reduction was monitored by a Balzers Omnistar200 mass spectrometer at $m/e = 44$.

2.3. Catalytic activity measurements

The catalytic activity of CO oxidation was evaluated in a fixed-bed reactor (6 mm i.d.) using 500 mg of catalyst (20–40 mesh). The total flow rate of the feed gas was 80 mL min^{-1}, corresponding to a space velocity (SV) of 9600 mL g^{-1} h^{-1}. The catalysts were directly exposed to reaction gas as the reactor temperature was stabilized at the reaction temperature without any pretreatment. For CO oxidation, a gas mixture consisted of 1% CO and 1% O_2 in N_2 with a total flow rate of 80 mL(NTP) min^{-1}. The reaction temperature was monitored by a thermocouple placed in the middle of the catalyst bed. The CO concentration in the reactor effluent was analyzed using an Agilent 6850 gas chromatograph equipped with a TCD detector attached to an HP PLOT column (30 m × 0.32 mm × 12 μm). For comparison, the reaction was carried out using 50 mg of

catalyst and a feed gas total flow rate of 100 mL min^{-1}, corresponding to an SV of 120,000 mL g^{-1} h^{-1}.

Catalytic tests for the selective oxidation of CO in excess hydrogen were carried out in a fixed-bed reactor (5 mm i.d.) at atmospheric pressure. A 50-mg sample of catalyst (60–80 mesh) was diluted with same amount of inert silicon dioxide. The gas consisted of 1% CO, 1% O_2, and 50% H_2 in Ar, with a total flow rate of 100 mL min^{-1}. The reactor inlet and outlet streams were measured by an on-line gas chromatograph equipped with a TCD and a flame ionization detector (FID). H_2, O_2, CO, and CO_2 were separated using a carbon molecular sieve (TDX-01) column. CO and CO_2 were converted to methane by a methanation reactor and analyzed using an FID. The carbon balance was close to $100 \pm 3\%$.

3. Results

3.1. Structural characterization

Fig. 1 shows the XRD patterns of the CuO–CeO_2 catalysts with different CuO contents. The distinct fluorite oxide diffraction pattern of CeO_2 is seen in all of the samples. However, XRD peaks due to CuO are not detected in the samples with low CuO content. At a CuO content of 28.3 mol%, weak diffraction peaks of CuO are seen; further increasing CuO content to 50.1 mol% causes an apparent increase in the intensities of the peaks.

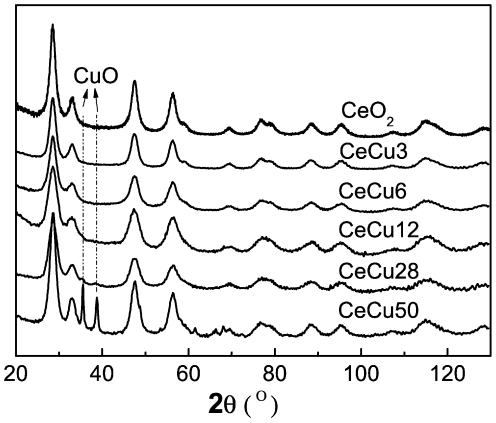

Fig. 1. XRD patterns of CuO–CeO_2 catalysts with different CuO contents.

The results of crystallite size and cell parameter measurements are summarized in Table 1. The table shows that cell parameter decreases with increasing CuO content up to 6.1 mol%, but remains almost constant between 12.0 and 50.1 mol%. A difference in the crystallite size of the directions (d_{111}, d_{200}, d_{220}) indicates the presence of anisotropy in the phase. In all samples, the crystallite size is <5 nm.

Fig. 2 shows the N_2 sorption isotherms and the pore size distributions of the CuO–CeO_2 catalysts with different CuO contents. The N_2 sorption isotherms of all samples (Fig. 2) are of type IV, typical of a mesoporous sample. The BET surface area and pore size of these samples are listed in Table 1. From Table 1 and Fig. 2, it can be seen that with increasing CuO content from 3.3 to 50.1 mol%, the BET surface areas of CuO–CeO_2 catalysts decrease from 215 to 91 m^2 g^{-1}, whereas the pore sizes increase from 6.4 to 17.8 nm.

Fig. 3 shows the TEM images of the sample CeCu6 and CeCu12. The images do not clearly show the presence of ordered mesopores, but reveal a rather foamlike structure resulting from closely aggregated metal oxide nanoparticles [24]. The size of the nanoparticles is around 5 nm, consistent with the crystallite size obtained by XRD.

3.2. Catalytic testing

Fig. 4 shows catalytic activities of CO oxidation over the CuO–CeO_2 catalysts at different SVs. It shows that the activ-

Table 1
Cell parameter, crystallite size, BET surface area and pore size of CeCu*x* catalysts

Sample	Cell parameter (nm)	Crystallite size (nm)			S_A (BET) (m^2 g^{-1})	Pore size (nm)
		$d(111)$	$d(200)$	$d(220)$		
CeCu0	0.5418(1)	4.58	4.41	4.54	202	6.6
CeCu3	0.5416(1)	4.89	4.89	4.89	215	6.4
CeCu6	0.5415(1)	3.40	3.54	3.49	180	7.1
CeCu12	0.5416(2)	3.21	3.41	3.27	150	9.6
CeCu28	0.5416(2)	3.88	3.71	3.24	116	11.2
CeCu50	0.5415(2)	5.10	4.56	4.27	91	17.8

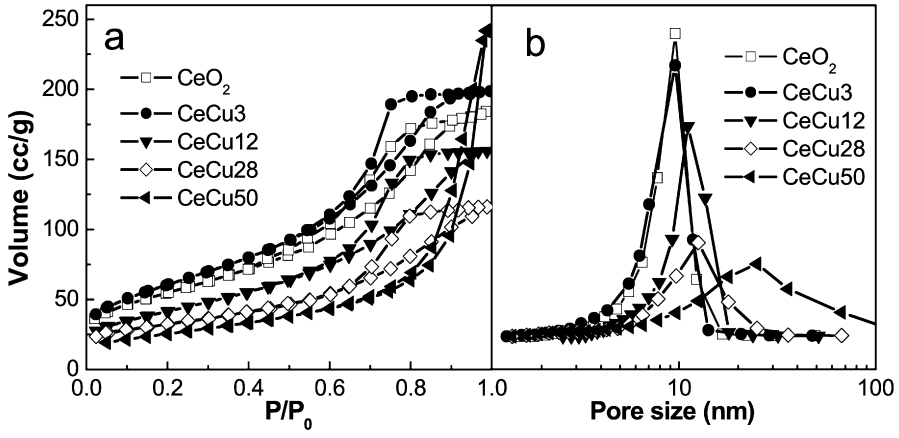

Fig. 2. N_2 sorption isotherms (a) and pore size distributions (b) of CuO–CeO_2 catalysts with different CuO contents.

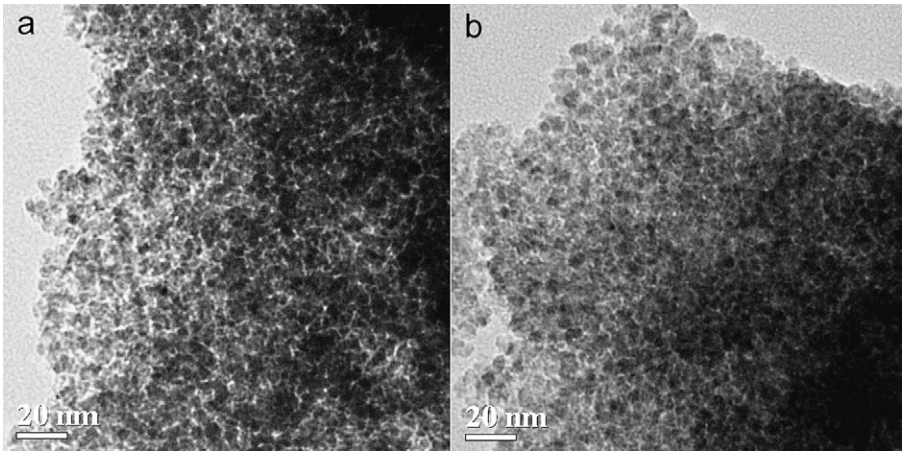

Fig. 3. TEM images of (a) CeCu6 and (b) CeCu12 catalysts.

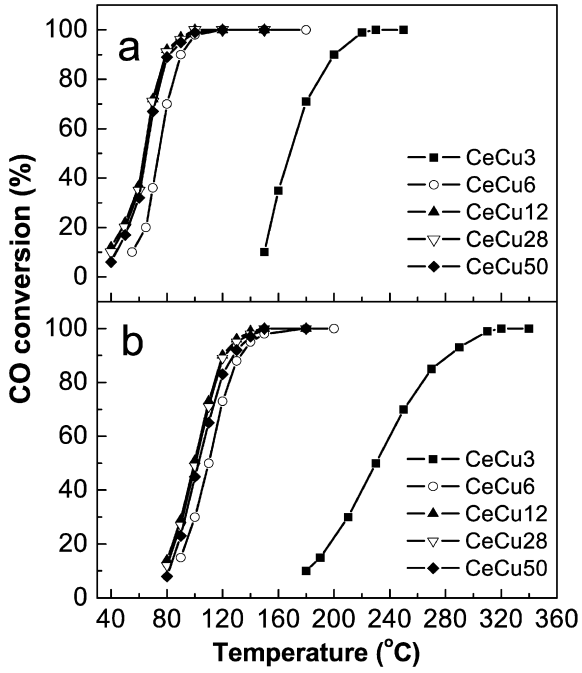

Fig. 4. CO oxidation over CeCux catalysts. (a) Space velocity = 9600 mL $g^{-1}\,h^{-1}$; (b) space velocity = 120,000 mL $g^{-1}\,h^{-1}$.

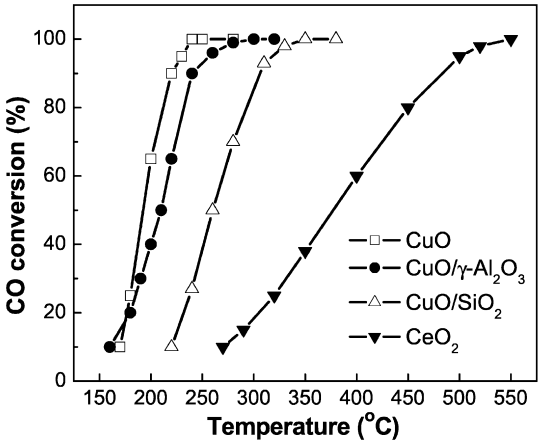

Fig. 5. CO oxidation over various CuO containing catalysts.

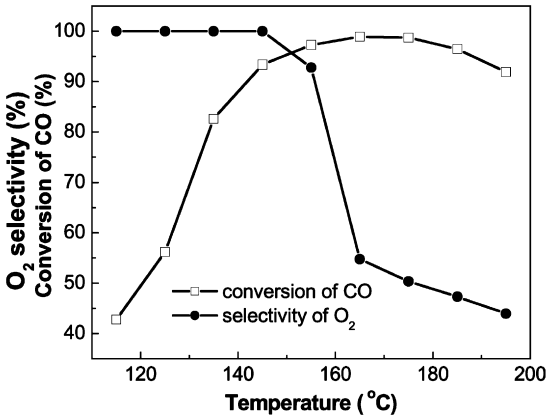

Fig. 6. CO oxidation in excess of H_2 over CeCu12 catalyst.

ity is significantly enhanced with increased CuO content in the catalyst. With increasing CuO content, T_{90} (the temperature for 90% conversion of CO) of the samples decreases sharply. The lowest T_{90} is 80 °C, achieved at the 12.0 mol% CuO content; T_{90} remains constant with increasing CuO content up to 50.1 mol%. For the same catalyst, it is seen that CO conversion is lower at high SV (120,000 mL $g^{-1}\,h^{-1}$) than at 9600 mL $g^{-1}\,h^{-1}$; this is because an increase in SV decreases the contact time with the catalyst.

For comparison, Fig. 5 shows the catalytic performance of the CuO/SiO_2 and $CuO/\gamma\text{-}Al_2O_3$ catalyst, as well as the pure CuO and CeO_2, on CO oxidation. It is seen that these catalysts are less active than the CuO–CeO_2 catalysts.

The catalytic performance of the CeCu12 catalyst for the selective oxidation of CO in excess H_2 was also investigated; the results are presented in Fig. 6. The CeCu12 catalyst is inactive for H_2 oxidation at reaction temperatures up to 145 °C. Therefore, 100% O_2 selectivity can be obtained over the CeCu12 catalyst at reaction temperatures below 145 °C, due to the lack of competitive oxidation of H_2. However, with a further increase in reaction temperature, H_2 oxidation reaction emerges, and the selectivity to O_2 decreases.

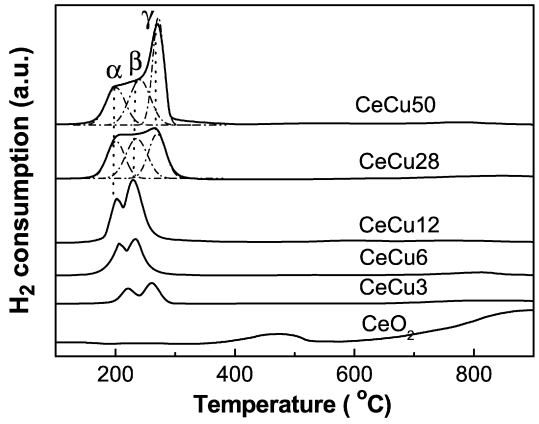

Fig. 7. H_2-TPR profiles of CuO–CeO_2 catalysts with different CuO contents.

3.3. TPR

TPR has been extensively used to characterize the reducibility of CuO–CeO_2 catalysts. H_2-TPR profiles of the CuO–CeO_2 catalysts and pure CeO_2 are shown in Fig. 7. The pure CeO_2 has two reduction peaks at about 450 and 900 °C, ascribed to the reduction of surface and bulk oxygen of CeO_2, respectively [25]. The profiles of all of the CuO–CeO_2 samples show two reduction peaks (α and β) in the range of 150–280 °C. As is well known, the reduction profile of pure CuO is characterized by a single peak at about 380 °C [14]. The H_2-TPR peak temperature of CuO–CeO_2 catalysts is much lower than that of pure CuO. With increasing CuO content from 3.3 to 12.0 mol%, the intensities of the peak α and β increase, and the peak positions shift to lower temperatures. With increasing CuO content up to 28.3 mol%, the peaks α and β coalesce and overlap, and a new peak, called γ, appears at 280 °C. With a further increase in CuO content to 50.1 mol%, the intensity of peak γ increases and the position shifts to higher temperature, but no visible changes occur in peaks α and β.

4. Discussion

In this work, a series of CuO–CeO_2 catalysts with CuO content of 3.3–50.1 mol% were prepared using a surfactant-templated method. The surface area was high, 91–215 $m^2\,g^{-1}$ (Table 1), higher than that for other reported Ce–Cu–O materials [19,20,25]. XRD (Fig. 1) showed no CuO diffraction peaks at lower CuO contents. This may be attributed to fine dispersion of CuO on the surface of CeO_2 [26], solid solution formation [27,28], or a combination of these two phenomena. The presence of CuO diffraction with high CuO content should be ascribed to bulk CuO. The cell parameter decreases with increasing CuO content up to 6.1 mol%, because the ionic radius of Cu^{2+} (0.072 nm) is smaller than that of Ce^{4+} (0.097 nm). When part of the CuO incorporates into the CeO_2 lattice and Cu^{2+} replaces Ce^{4+}, a reduction in the cell parameter of ceria occurs. Therefore, changes in the cell parameter of the catalysts (Table 1) indicate that the missing CuO phase in XRD at low CuO content may have partly formed a $Cu_xCe_{1-x}O_{2-\delta}$ solid solution [29,30].

The N_2 sorption experiments show that all of the samples are porous. However, the lack of low-angle XRD peaks indicates they do not have regularly ordered mesoporous pores. This is also consistent with the TEM observations (Fig. 3). In addition, with increasing CuO content of the catalysts, formation of the bulk CuO results in decreased BET surface area and, consequently, increased pore size.

The CuO–CeO_2 catalysts reported in this work have slightly higher catalytic activities than other reported Cu-modified or -doped cerium oxide materials for the oxidation of CO to CO_2 at relatively low temperatures [19,20,25]. Tang et al. [25] reported the synthesis of a CuO–CeO_2 (10 wt% Cu) catalyst by a co-precipitation method. The T_{90} for the CO oxidation reaction of this catalyst was about 90 °C with an SV of 10,000 ml g^{-1} h^{-1}. In the present work, the T_{90} of the CO reaction over the CeCu12 catalyst is about 80 °C with almost the same SV (Fig. 4a). The decline in T_{90} of the catalysts with different CuO contents (Fig. 4a) implies that the CuO species should be responsible for the activity. In the H_2-TPR results for the catalysts, all profiles show peak α and peak β. We previously reported two reduction peaks of H_2-TPR [14], with the peak α ascribed to finely dispersed CuO and the peak β assigned to the larger particles of the bulk CuO. The same results also have been reported by Kundakovic and Flytzani-Stephanopoulos [31]. However, in H_2-TPR of the present work (Fig. 7), the peaks α and β coexist in all TPR profiles even at 1.5 mol% CuO content, and the area of peak β always larger than that of peak α. In the meantime, the XRD results show that part of the Cu^{2+} ions replaces Ce^{4+} to form a $Cu_xCe_{1-x}O_{2-\delta}$ solid solution at low CuO content. Therefore, it is more likely that peak α is due to the reduction of finely dispersed CuO and peak β is due to the reduction of Cu^{2+} ions in $Cu_xCe_{1-x}O_{2-\delta}$ solid solution. In addition, with further increases in CuO content up to 28.3 mol%, the bulk CuO becomes present in the sample (Fig. 1), and a new peak γ is found by H_2-TPR, suggesting that this peak γ is due to the reduction of bulk CuO.

It is commonly believed that the finely dispersed CuO is the active phase for CO oxidation [14]. Therefore, the activity should decrease if the active phase is removed. The finely dispersed CuO particles can be easily dissolved in nitric acid [14]. In this work, the CeCuO12 catalyst was immersed in concentrated nitric acid (15 ml of 50% HNO_3/g catalyst) for 2 h, filtered, then washed with plenty of distilled water to remove the residual HNO_3 or other impurities, and dried at 120 °C. This catalyst was designated as CeCu12-H. This catalyst's CuO content was 8.1 mol% by AAS analysis. After the acid treatment, its BET surface area increased from 150 to 172 $m^2\,g^{-1}$, suggesting that removing the finely dispersed CuO species produced an increase in surface area. However, the cell parameter and crystallite size were 0.5416(2) nm and 3.16 nm, respectively, with no visible changes seen compared with the untreated sample (Table 1). CO oxidation activities of the CeCuO12 catalyst and the CeCu12-H catalyst are shown in Fig. 8. The catalytic activity evidently drops after the acid treatment.

H_2-TPR profiles of the CeCuO12 catalyst and CeCu12-H catalyst are shown in Fig. 9a. The figure shows that the peak α

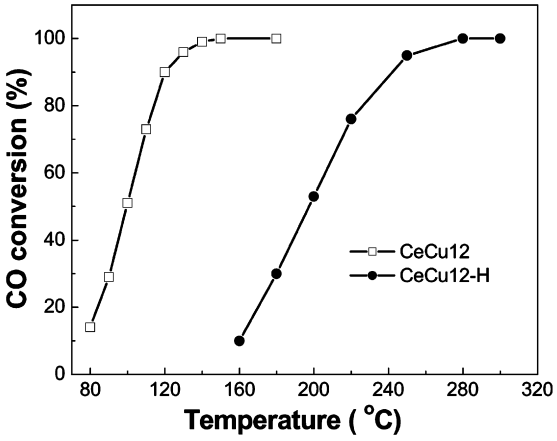

Fig. 8. CO oxidation over CeCu12 and CeCu12-H at a space velocity of 120,000 mL g^{-1} h^{-1}.

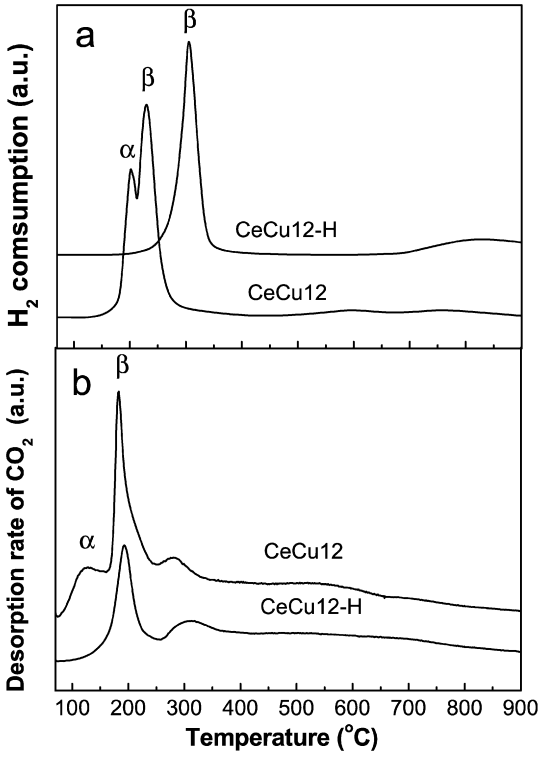

Fig. 9. H_2-TPR profiles (a) and CO-TPR profiles (b) of CeCu12 and CeCu12-H samples.

of CeCu12 disappears after the acid treatment, indicating that the finely dispersed CuO species are the active sites for CO oxidation, and also shows that peak β is represented by Cu^{2+} incorporating into the CeO_2 lattice. However, in Fig. 9a, the position of the peak β shifts to higher temperature after acid treatment. To explain this shift in peak β, CO-TPR was carried out on the CeCu12-H and CeCu12 samples; the profiles are also presented in Fig. 9b. After acid treatment, the peak α of CeCu12 disappears, but the peak β remains consistent, in contrast to the H_2-TPR findings. The difference between H_2-TPR and CO-TPR can be explained by the following mechanism. In H_2-TPR, due to hydrogen spillover [32], when the finely dispersed CuO of CeCu12 sample is reduced, the atomic hydrogen

Table 2
Comparison of Cu content before and after nitric acid treatment

Sample	Cu/(Cu + Ce) (mol%)	
	Nominal	XPS
CeCu12	12.0	23.7
CeCu12-H	8.1	8.7

generated by dissociative adsorption on the metallic Cu surface can spill over onto the surface of the lattice Cu^{2+}, thereby decreasing its reduction temperature. After the finely dispersed CuO is removed by acid treatment, the reduction temperature of peak β evidently increases. However, in CO-TPR, the carbon monoxide spillover effect does not exist; thus, the position of peak β remains constant before and after acid treatment. A weak peak is present at about 300 °C in Fig. 9b. It is evident that the temperatures of the reduction peaks of CO-TPR are lower than those of H_2-TPR. Therefore, we believe that the reduction peak of CO-TPR seen at about 300 °C is probably due to reduction of some of the CeO_2 surface oxygen.

To further clarify the surface changes caused by the acid treatment, XPS analysis was conducted. Table 2 summarizes the surface concentrations of Cu before and after the acid treatment. Clearly, that for the untreated sample, the surface Cu concentration (23.7%) is much higher than the nominal one (12.0%), due to the aggregation of the CuO species on the surface. In contrast, after acid treatment, the surface Cu concentration (8.7%) is close to the nominal one (8.1%), indicating complete removal of the surface CuO species. These results are in good agreement with the H_2-TPR and the CO-TPR results, strongly suggesting that the surface CuO species are responsible for CO oxidation, and that the decreased activity is due to the removal of surface CuO species.

High catalytic activity of the CeCu12 catalyst for selective oxidation of CO in excess H_2 at lower temperature is understandable. Comparing Figs. 9a and 9b clearly shows that the reduction temperature (120 °C) of the finely dispersed CuO is lower in CO than in H_2 (200 °C), indicating that the reaction of CO is easier than that of H_2. These findings may relate to the CO selectivity of the CuO–CeO_2 catalyst in excess H_2. At the same SV, the activity for CO oxidation in excess H_2 (Fig. 6) is slightly lower than that in CO atmosphere alone (Fig. 4b). This may be due to the competitive adsorption of H_2 and CO on the active sites.

In addition, to prove the influence of the surface area on the catalytic activity, the CO oxidation activities of Cu–Ce–O catalysts with similar CuO contents but different surface areas were tested. The results are shown in Fig. 10, and the BET surface areas, calculated average crystallite sizes, and cell parameters are given in Table 3. The CuO content is 10 mol% in the N8A4, A4, and A8 samples. Fig. 4 shows that the CuCe6 and the CuCe12 samples have similar catalytic activity; thus, if a CuCe10 sample does exist, then its catalytic activity should be close to that of CuCe12. It can be seen that the larger the surface area, the greater the catalytic activity. The CuCe12 catalyst has the largest surface area (150 m^2 g^{-1}) and greatest catalytic activity. This is because increasing the surface area of the cat-

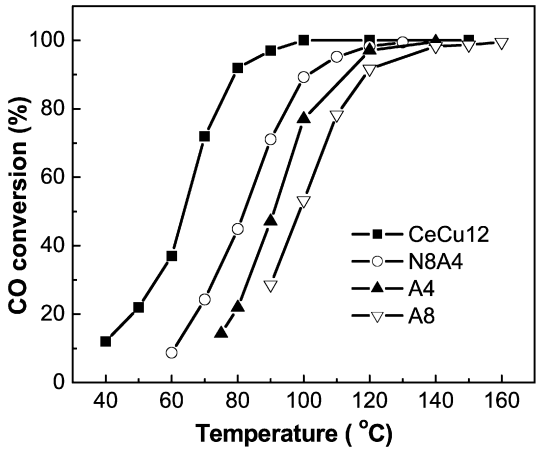

Fig. 10. CO oxidation over Cu–Ce–O catalysts with similar CuO content but different surface areas.

Table 3
Cell parameter, crystallite size and BET area of different Ce–Cu–O catalysts

Sample	Cell parameter (nm)	Crystallite size (nm)			S_A (BET) ($m^2\ g^{-1}$)
		$d(111)$	$d(200)$	$d(220)$	
CeCu12	0.5416(2)	3.21	3.41	3.27	150
N8A4	0.5418(2)	6.95	6.87	6.89	131
A4	0.5419(1)	8.08	8.10	8.09	60
A8	0.5418(1)	6.36	6.36	6.36	10

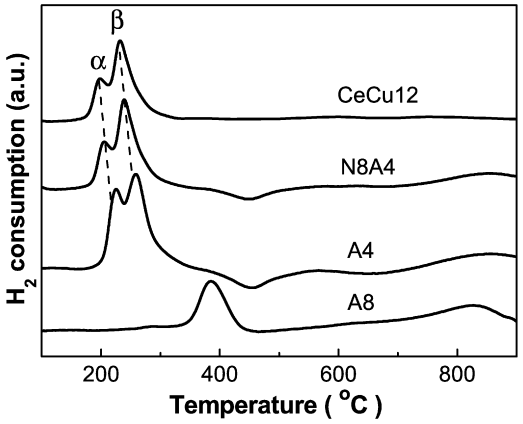

Fig. 11. H_2-TPR profiles of CuCe12, N8A4, A4 and A8 catalysts.

alyst aids the formation of the finely dispersed CuO. Fig. 11 shows H_2-TPR profiles of the CuCe12 and N8A4, A4, and A8 catalysts. These profiles demonstrate that the peak α shifts toward lower temperature with increasing surface area. This may be due to the CuO dispersion state becoming finer and the CuO crystallite becoming smaller [30] with increasing surface area of the catalyst. Therefore, there are more exposed active sites on the high-surface area catalysts than on the low-surface area catalysts, which could explain the difference in the CO oxidation activity.

5. Conclusion

The surfactant-templated method presented in this work has allowed us to prepare high-surface area nanosized CuO–CeO_2 catalysts. Higher CO oxidation activities of the catalysts were obtained compared with samples with low surface areas. H_2-TPR suggests the presence of three different CuO species: highly dispersed CuO, Cu^{2+} in the CeO_2 lattice, and bulk CuO species. The activity of the catalyst for CO oxidation obviously declined after the removal of highly dispersed CuO by acid treatment, indicating that the highly dispersed CuO species are the active phase for CO oxidation.

Acknowledgments

This work was supported by the Natural Science Foundation of China (grant 20473075) and the Zhejiang Provincial Nature Science Foundation of China (grant Z404383). The authors thank Professor Guang-Lie Lv (Zhejiang University, China) for calculating the microstructural parameters and Dr. Zhi-Gang Liu (Zhejiang University, China) for carrying out the selective oxidation of CO in excess H_2.

References

[1] N. Izu, W. Shin, N. Murayama, S. Kanzaki, Sens. Actuators B 87 (2002) 95.
[2] A. Martínez-Arias, M. Fernández-García, O. Gálvez, J.M. Coronado, J.A. Anderson, J.C. Conesa, J. Soria, G. Munuera, J. Catal. 195 (2000) 207.
[3] X. Wang, J.A. Rodriguez, J.C. Hanson, D. Gamarra, A. Martínez-Arias, M. Fernández-García, J. Phys. Chem. B 110 (2006) 428.
[4] P. Bera, K.C. Patil, V. Jayaram, G.N. Subbanna, M.S. Hegde, J. Catal. 196 (2000) 293.
[5] F. Mariño, C. Descorme, D. Duprez, Appl. Catal. B 54 (2004) 59.
[6] C.N. Costa, S.Y. Christou, G. Georgiou, A.M. Efstathiou, J. Catal. 219 (2003) 259.
[7] P.G. Harrison, I.K. Ball, W. Azalee, W. Daniell, D. Goldfarb, Chem. Mater. 12 (2000) 3715.
[8] S. Hočevar, U.O. Krasovec, B. Orel, A.S. Arico, H. Kim, Appl. Catal. B 28 (2000) 113.
[9] P.-O. Larsson, A. Andersson, Appl. Catal. B 24 (2000) 175.
[10] A. Martínez-Arias, M. Fernández-García, J. Soria, J.C. Conesa, J. Catal. 182 (1999) 367.
[11] C.R. Jung, J. Han, S.W. Nam, T.-H. Lim, S.-A. Hong, H.-I. Lee, Catal. Today 93–95 (2004) 183.
[12] P. Bera, S.T. Aruna, K.C. Patil, M.S. Hegde, J. Catal. 186 (1999) 36.
[13] M. Jobbágy, M. Fernando, B. Schönbrod, G. Baronetti, M. Laborde, Chem. Mater. 18 (2006) 1945.
[14] M.F. Luo, Y.J. Zhong, X.X. Yuan, X.M. Zheng, Appl. Catal. A 162 (1997) 121.
[15] S.D. Gardner, G.B. Hoflund, B.T. Upchurch, D.R. Schryer, E.J. Kielin, J. Schryer, J. Catal. 129 (1991) 114.
[16] L. Yin, Y. Wang, G. Pang, Y. Koltypin, A. Gedanken, J. Colloid Interface Sci. 246 (2002) 78.
[17] M. Hirano, M. Inagaki, J. Mater. Chem. 10 (2000) 473.
[18] A.I.Y. Tok, L.H. Luo, F.Y.C. Boey, Mater. Sci. Eng. A 383 (2004) 229.
[19] B. Skårman, D. Grandjean, R.E. Benfield, A. Hinz, A. Andersson, L.R. Wallenberg, J. Catal. 211 (2002) 119.
[20] W. Shen, X. Dong, Y. Zhu, H. Chen, J. Shi, Microporous Mesoporous Mater. 85 (2005) 157.
[21] G.Q. Xie, M.F. Luo, M. He, P. Fang, J.M. Ma, Y.F. Ying, Z.L. Yan, J. Nanopart. Res. (2006) 3, online.
[22] R.A. Young, The Rietveld Method, Oxford Univ. Press, Oxford, UK, 1993.
[23] L. Lutterotti, S. Gialanella, Acta Mater. 46 (1998) 101.
[24] A.K. Sinha, K. Suzuki, J. Phys. Chem. B 109 (2005) 1708.
[25] X. Tang, B. Zhang, Y. Li, Y. Xu, Q. Xin, W. Shen, Catal. Today 93–95 (2004) 191.
[26] S.-M. Zhang, W.-P. Huang, X.-H. Qiu, B.-Q. Li, X.-C. Zheng, S.-H. Wu, Catal. Lett. 80 (2002) 41.

[27] C. Lamonier, A. Ponchel, A. D'Huysser, L. Jalowiecki-Duhamel, Catal. Today 50 (1999) 247.
[28] P. Bera, K.R. Priolkar, P.R. Sarode, M.S. Hegde, S. Emura, R. Kumashiro, N.P. Lalla, Chem. Mater. 14 (2002) 3591.
[29] Y. Li, Q. Fu, M. Flytzani-Stephanopoulos, Appl. Catal. B 27 (2000) 179.
[30] X. Jiang, G. Lu, R. Zhou, J. Mao, Y. Chen, X. Zheng, Appl. Surf. Sci. 173 (2001) 208.
[31] L. Kundakovic, M. Flytzani-Stephanopoulos, Appl. Catal. A 171 (1998) 13.
[32] R. Kramer, M. Andre, J. Catal. 58 (1979) 287.